Chapter 5

Thick Plates

5.1 Introduction

This chapter deals with the application of T-elements to thick plate problems. In contrast to Kirchhoff's thin plate theory, the transverse shear deformation effect of the plate is taken into account in thick plate theory, so that the governing equation is a sixth-order boundary value problem. As a consequence, three boundary conditions should be considered for each boundary. In contrast, Only two boundary conditions are considered in thin plate theory.

It is well-known that Kirchhoff's thin plate theory [25] demands both the deflection and normal rotations to be continuous between elements, i.e., C^1 continuous. This requirement makes it difficult to construct conforming elements. This difficulty can be bypassed using thick plate theory, usually Mindlin's theory [12] which is based on independent approximations for the deflections and rotations. Elements based on Mindlin's theory require only C^0 continuity, which is readily achieved. Moreover, the theory is applicable to both thick and thin plates [11]. Despite these advantages, there are a number of problems associated with thick plate elements. Specifically, the elements can lock as the plate thickness approaches zero, thereby giving incorrect results for thin plates. In addition, many elements have zero energy modes, which may cause spurious mechanisms to spread through the mesh. Many techniques, such as reduced integration, special shear interpolation and stabilization matrix, have been used to alleviate these problems. It has been shown that the use of hybrid-Trefftz thick plate elements can also eliminate these problems [10,11]. Based on the Trefftz method, Petrolito [14,15] presented a hierarchic family of triangular and quadrilateral T-elements for analyzing moderately thick Reissner-Mindlin plates. In these HT formula-tions, the displacement and rotation components of the auxiliary frame field $\tilde{\mathbf{u}} = \{\tilde{w}, \tilde{\psi}_x, \tilde{\psi}_y\}^T$, where ψ_i is defined in eqn (1.76), used to enforce conformity on the internal Trefftz field $\mathbf{u} = \{w, \psi_x, \psi_y\}^T$, are independently interpolated along the element boundary in terms of nodal values. Jirousek *et al*. [11] showed that the performance of the HT thick plate elements could be considerably improved by the application of a linked interpolation whereby the boundary interpolation of the displacement, $\tilde{w}$, is linked through a suitable constraint with that of the tangential rotation component, $\tilde{\psi}_s$. This concept, introduced in [23], has been recently applied by several researchers to develop simple and well-performing thick plate elements [1,5,10,11,22,24,26].

Practical experience with existing HT-elements for thin plates [6] and plane elasticity [9] has clearly shown that, from the point of view of cost and convenience of use, the convergence based on *p*-extension is largely preferable to the more conventional *h*-refinement process [8]. From the discussion in the

previous chapters, it can be seen that, in the HT FE approach, *p*-extension implies the representation of the intra-element displacement field which is based on a T-complete set of Trefftz functions. Use of such a set warrants that under very general conditions, the approximation converges towards the exact solution if the number of functions is increased (for a rigorous definition of T-completeness see, e.g. [3]). Unfortunately, the set of polynomial Trefftz functions, as introduced in [14] for thick plate application, is not T-complete and, as a consequence, convergence of the *p*-extension process toward the exact solution cannot be assured. In practice it means that the question of whether the process of increasing the order of approximation of the elements results in improvement or deterioration of the solution is problem dependent. In particular, if the tangential component $\tilde{\psi}_s$ of the rotation at the plate boundary is unconstrained (soft simple support or free edge), then the *p*-extension may diverge if the internal set of Trefftz functions is not T-complete. To solve this problem, we developed a new family of quadrilateral HT *p*-elements for thick plate analysis [10]. In this work, the incomplete set of Trefftz functions introduced in [14] was replaced by a T-complete set, and the linked interpolation concept [23] was extended from the lowest elements to the higher order elements. Recently, Qin [17-19] extended this approach to the analysis of thick plates on elastic foundation and to the nonlinear thick plate problem.

In this chapter we start with a brief review on thick plate theory followed by the derivation of element stiffness equations. At the end of this chapter, a critical numerical assessment is performed to demonstrate performance of various types of hybrid-Trefftz thick plate elements.

5.2 Basic equations for Reissner-Mindlin plate theory

The HT FE formulation derived in this chapter is based on the customary theory of moderately thick plates with transverse shear deformation [12,21]. In contrast to thin plate theory as described in the previous chapter, Reissner-Mindlin theory [12,21] incorporates the contribution of shear deformation to the transverse deflection. In Reissner-Mindlin theory, it is assumed that the transverse deflection of the middle surface is *w*, and that straight lines initially normal to the middle surface rotate ψ_x about the *y*-axis and ψ_y about the *x*-axis (see Fig. 4.3). The variables (w, ψ_x, ψ_y) are considered to be independent variables and to be functions of *x* and *y* only. A convenient matrix form of the resulting relations of this theory may be obtained through use (Figs. 4.2 and 4.3) of the following matrix quantities:

$$\mathbf{u} = \{w, \psi_x, \psi_y\}^T, \qquad \text{(generalized displacement)}, \tag{5.1}$$

$$\boldsymbol{\varepsilon} = \{\chi_x\ \chi_y\ \chi_{xy}\ \gamma_x\ \gamma_y\}^T = \mathbf{L}^T\mathbf{u}, \qquad \text{(generalized strains)}, \tag{5.2}$$

$$\boldsymbol{\sigma} = \{-M_x\ -M_y\ -M_{xy}\ Q_x\ Q_y\}^T = \mathbf{D}\boldsymbol{\varepsilon}, \qquad \text{(generalized stresses)}, \tag{5.3}$$

$$\mathbf{t} = \{Q_n - M_{nx} - M_{ny}\}^T = \mathbf{A}\boldsymbol{\sigma}, \quad \text{(generalized boundary tractions)}, \tag{5.4}$$

where **L**, **D** and **A** are defined in eqn (1.76).

The governing differential equations of moderately thick plates are obtained if the differential equilibrium conditions are written in terms of **u** as

$$\mathbf{L}\boldsymbol{\sigma} = \mathbf{L}\mathbf{D}\mathbf{L}^T\mathbf{u} = \overline{\mathbf{b}}, \tag{5.5}$$

where the load vector

$$\overline{\mathbf{b}} = \{\overline{q}\ \overline{m}_x\ \overline{m}_y\}^T, \tag{5.6}$$

comprises the distributed vertical load in the z direction and the distributed moment loads about the y and x axes (the bar above the symbols indicates imposed quantities).

The corresponding boundary conditions are given by

(a) *natural boundary conditions*

$$M_n = M_{ij}n_i n_j = \overline{M}_n, \qquad (\text{on } \Gamma_{M_n}), \tag{5.7}$$

$$M_{ns} = M_{ij}n_i s_j = \overline{M}_{ns}, \qquad (\text{on } \Gamma_{M_{ns}}), \tag{5.8}$$

$$Q_n = Q_i n_i = \overline{Q}_n, \qquad (\text{on } \Gamma_Q). \tag{5.9}$$

(b) *essential boundary conditions*

$$\psi_n = \psi_i n_i = \overline{\psi}_n, \qquad (\text{on } \Gamma_{\psi_n}), \tag{5.10}$$

$$\psi_s = \psi_i s_i = \overline{\psi}_s, \qquad (\text{on } \Gamma_{\psi_s}), \tag{5.11}$$

$$w = \overline{w}, \qquad (\text{on } \Gamma_w), \tag{5.12}$$

where n and s are, respectively, unit vectors outward normal and tangent to the plate boundary Γ ($\Gamma = \Gamma_{\psi_n} \cup \Gamma_{M_n} = \Gamma_{\psi_s} \cup \Gamma_{M_{ns}} = \Gamma_w \cup \Gamma_Q$).

5.3 Assumed fields and particular solution

5.3.1 Internal field

The internal displacement field in a thick plate element is assumed as

$$\mathbf{u} = \{w, \psi_x, \psi_y\}^T = \breve{\mathbf{u}} + \sum_{j=1}^{m} \mathbf{N}_j \mathbf{c}_j = \breve{\mathbf{u}} + \mathbf{N}\mathbf{c}, \tag{5.13}$$

where $\mathbf{c}_j$ stands for undetermined coefficients and $\breve{\mathbf{u}}$ and $\mathbf{N}_j$ are, respectively,

the particular and homogeneous solutions to the governing differential equations (5.5), namely,

$$\mathbf{LDL}^T\breve{\mathbf{u}} = \overline{\mathbf{b}} \quad \text{and} \quad \mathbf{LDL}^T\mathbf{N}_j = 0\,, \qquad (j = 1,2,\cdots,m)\,. \tag{5.14}$$

To generate the internal function $\mathbf{N}_j$, consider again the governing equations (5.5) and write them in a convenient form as

$$D\left[\frac{\partial^2\psi_x}{\partial x^2} + \frac{1-\mu}{2}\frac{\partial^2\psi_x}{\partial y^2} + \frac{1+\mu}{2}\frac{\partial^2\psi_y}{\partial x\partial y}\right] + C\left(\frac{\partial w}{\partial x} - \psi_x\right) = 0\,, \tag{5.15}$$

$$D\left[\frac{\partial^2\psi_y}{\partial y^2} + \frac{1-\mu}{2}\frac{\partial^2\psi_y}{\partial x^2} + \frac{1+\mu}{2}\frac{\partial^2\psi_x}{\partial x\partial y}\right] + C\left(\frac{\partial w}{\partial y} - \psi_y\right) = 0\,, \tag{5.16}$$

$$C\left(\nabla^2 w - \frac{\partial\psi_x}{\partial x} - \frac{\partial\psi_y}{\partial y}\right) = \overline{q}\,, \tag{5.17}$$

where

$$D = \frac{Et^3}{12(1-\mu^2)}, \quad C\frac{5Et}{12(1+\mu)}\,, \tag{5.18}$$

and where, for the sake of simplicity, vanishing distributed moment loads, $\overline{m}_x = \overline{m}_y = 0$, have been assumed.

The coupling of the governing differential equations (5.15)-(5.17) makes it difficult to generate a T-complete set of homogeneous solutions for w, ψ_x and ψ_y. To bypass this difficulty, two auxiliary functions f and g are introduced such that [4]

$$\psi_x = g_{,x} + f_{,y} \quad \text{and} \quad \psi_y = g_{,y} - f_{,x}\,. \tag{5.19}$$

It should be pointed out that

$$g_{0,x} + f_{0,y} = 0 \quad \text{and} \quad g_{0,y} - f_{0,x} = 0\,, \tag{5.20}$$

are Cauchy-Riemann equations, the solution of which always exists. As a consequence, ψ_x and ψ_y remain unchanged if f and g in eqn (5.19) are replaced by $f + f_0$ and $g + g_0$. This property will play an important role in the subsequent derivation.

The solution of eqn (5.20) may be conveniently expressed in a complex variable form (with $i = \sqrt{-1}$) as

$$f_0 + ig_0 = \Phi(x+iy)\,. \tag{5.21}$$

The substitution of eqn (5.19) into eqns (5.15) and (5.16) yields

$$\frac{\partial}{\partial x}[D\nabla^2 g + C(w-g)] + \frac{\partial}{\partial y}\left[\frac{1}{2}D(1-\mu)\nabla^2 f - Cf\right] = 0\,, \tag{5.22}$$

$$\frac{\partial}{\partial y}[D\nabla^2 g + C(w-g)] - \frac{\partial}{\partial x}\left[\frac{1}{2}D(1-\mu)\nabla^2 f - Cf\right] = 0\,. \tag{5.23}$$

Now, if the contents of the two brackets are considered as independent generalized variables,

$$A = \left[\frac{1}{2}D(1-\mu)\nabla^2 f - Cf\right] \quad \text{and} \quad B = [D\nabla^2 g + C(w-g)]\,, \tag{5.24}$$

we again get a set of Cauchy-Riemann equations

$$B_{,x} + A_{,y} = 0 \quad \text{and} \quad B_{,y} - A_{,x} = 0\,, \tag{5.25}$$

and, in the same manner as in eqn (5.21), we can get

$$A + iB = \left[\frac{1}{2}D(1-\mu)\nabla^2 f - Cf\right] + i[D\nabla^2 g + C(w-g)] = F(x+iy)\,. \tag{5.26}$$

This relation is a non-homogeneous equation with independent unknown functions *f*, *g* and *w*. Its solution can be composed of a particular solution and a homogeneous solution. Since $F(x+iy)$ is a harmonic function, it is easy to see that the particular solution can be taken as

$$f + ig = -\frac{1}{C}F(x+iy) \quad \text{and} \quad w=0. \tag{5.27}$$

It is obvious, with reference to eqns (5.19) and (5.20), that this solution leads to $w = \psi_x = \psi_y = 0$. Therefore, the particular solution may simply be omitted and we need to consider only the homogeneous part of eqn (5.26), namely

$$\left[\frac{1}{2}D(1-\mu)\nabla^2 f - Cf\right] = 0 \quad \text{and} \quad D\nabla^2 g + C(w-g) = 0\,. \tag{5.28}$$

From the second of these equations, we have

$$w = g - \frac{D}{C}\nabla^2 g\,. \tag{5.29}$$

The substitution of this relation and of the expressions (5.19) into eqn (5.17) finally leads to

$$D\nabla^4 g = \overline{p}\,. \tag{5.30}$$

As a result, we obtain for g and f the following differential equations

$$D\nabla^4 g = \overline{p} \quad \text{and} \quad \nabla^2 f - \lambda^2 f = 0\,, \tag{5.31}$$

with $\lambda^2 = 10(1-\mu)/t^2$.

The relations (5.31) are the biharmonic equation and the modified Bessel equation, respectively. Their T-complete solutions have been provided in eqn (4.30) for the former and in eqn (4.104) for the latter. Thus the series for f and g can be taken as

$$f_1 = I_0(\lambda r), \quad f_{2k} = I_k(\lambda r)\cos k\theta\,, \quad f_{2k+1} = I_k(\lambda r)\sin k\theta \qquad k = 1,2,\cdots, \tag{5.32}$$

$$g_1 = r^2, \quad g_2 = x^2 - y^2\,, \quad g_3 = xy\,, \quad g_{4k} = r^2 \operatorname{Re} z^k\,,$$

$$g_{4k} = r^2 \operatorname{Im} z^k\,, \quad g_{4k+2} = \operatorname{Re} z^{k+2}\,, \quad g_{4k+3} = \operatorname{Im} z^{k+2} \qquad k = 1,2,\cdots. \tag{5.33}$$

In agreement with relations (5.19) and (5.29), the homogeneous solutions w_i, ψ_{xi}, ψ_{yi} are obtained in terms of g's and f's as

$$w_i = g - \frac{D}{C}\nabla^2 g\,, \quad \psi_{xi} = g_{,x} + f_{,y}\,, \quad \psi_{yi} = g_{,y} - f_{,x}\,. \tag{5.34}$$

However, since sets of functions f_k (5.32) and functions g_j (5.33) are independent of each other, the sub-matrices $\mathbf{N}_i = \{w_i, \psi_{xi}, \psi_{yi}\}^T$ in eqn (5.13) will be of the following two types:

$$\mathbf{N}_i = \begin{Bmatrix} g_j - \dfrac{D}{C}\nabla^2 g_j \\ g_{j,x} \\ g_{j,y} \end{Bmatrix}, \tag{5.35}$$

or

$$\mathbf{N}_i = \begin{Bmatrix} 0 \\ f_{k,y} \\ -f_{k,x} \end{Bmatrix}. \tag{5.36}$$

One of the possible methods of relating index i to corresponding j or k values in eqn (5.35) or (5.36) is displayed in Table 5.1. However, many other possibilities exist [17]. It should also be pointed out that successful h-method elements have been obtained in [11,14] with only polynomial set of homogeneous solutions.

Table 5.1. Examples of ordering of indexes *i*, *j* and *k* appearing in eqns (5.35) and (5.36).

i	1	2	3	4	5	6	7	8	9	10	11	12	13	14	15	16	17
j	1	2	3	4	5	-	6	7	8	9	-	-	10	11	12	13	-
k	-	-	-	-	-	1	-	-	-	-	2	3	-	-	-	-	4

i	18	19	20	21	22	23	24	25	26	27	28	29	…	etc.
j	-	14	15	16	17	-	-	18	19	20	21	-	…	etc.
k	5	-	-	-	-	6	7	-	-	-	-	8	…	etc.

5.3.2 Particular solution $\breve{\mathbf{u}} = \{\breve{w}, \breve{\psi}_x, \breve{\psi}_y\}^T$

The effect of various loads can accurately be accounted for by a particular solution of the form

$$\breve{\mathbf{u}} = \begin{Bmatrix} \breve{w} \\ \breve{\psi}_x \\ \breve{\psi}_y \end{Bmatrix} = \begin{Bmatrix} \breve{g} - \dfrac{D}{C}\nabla^2 \breve{g} \\ \breve{g}_{,x} \\ \breve{g}_{,y} \end{Bmatrix}, \tag{5.37}$$

where $\breve{g}$ is a particular solution of eqn (5.30). The most useful solutions are

$$\breve{g} = \frac{\bar{q} r^4}{64D}, \tag{5.38}$$

for a uniform load $\bar{q} = \text{constant}$, and

$$\breve{g} = \frac{\bar{P} r_{PQ}^2}{8\pi D} \ln r_{PQ}, \tag{5.39}$$

for a concentrated load $\bar{P}$, where r_{PQ} is defined in Section 2.4. A number of particular solutions for Reissner-Mindlin plates can be found in standard texts, e.g. [20].

5.3.3 Frame field

Since evaluation of the element matrices calls for boundary integration only (see Section 4.6, for example), explicit knowledge of the domain interpolation of the auxiliary conforming field is not necessary. As a consequence the boundary distribution of $\tilde{\mathbf{u}} = \tilde{\mathbf{N}}\mathbf{d}$, referred to as 'frame function', is all that is needed.

The elements considered in this chapter are either *p*-type ($M \neq 0$) (Fig. 1.3) or conventional-type (M=0), with 3 standard DOF at corner nodes, e.g.,

$$\mathbf{d}_A = \tilde{\mathbf{u}}_A = \{\tilde{w}_A, \tilde{\psi}_{xA}, \tilde{\psi}_{yA}\}^T \ , \quad \mathbf{d}_B = \tilde{\mathbf{u}}_B = \{\tilde{w}_B, \tilde{\psi}_{xB}, \tilde{\psi}_{yB}\}^T \ , \tag{5.40}$$

and an optional number, *M*, of hierarchical DOF associated with mid side nodes

$$\mathbf{d}_C = \Delta\tilde{\mathbf{u}}_C = \{\Delta\tilde{w}_{C1}, \Delta\tilde{\psi}_{xC1}, \Delta\tilde{\psi}_{yC1}, \Delta\tilde{w}_{C2}, \Delta\tilde{\psi}_{xC2}, \Delta\tilde{\psi}_{yC2}, \cdots \text{etc.}\}^T \ . \tag{5.41}$$

Within the thin limit $\tilde{\psi}_x = \partial\tilde{w}/\partial x$ and $\tilde{\psi}_y = \partial\tilde{w}/\partial y$, the order of the polynomial interpolation of $\tilde{w}$ has to be one degree higher than that of ψ_x and ψ_y if the resulting element is to be free of shear locking. Hence, if along a particular side A-C-B of the element (Fig. 1.3)

$$\tilde{\psi}_{xA-C-B} = \tilde{N}_A\tilde{\psi}_{xA} + \tilde{N}_B\tilde{\psi}_{xB} + \sum_{i=1}^{\tilde{p}-1}\tilde{N}_{Ci}\Delta\tilde{\psi}_{xCi} \ , \tag{5.42}$$

$$\tilde{\psi}_{yA-C-B} = \tilde{N}_A\tilde{\psi}_{yA} + \tilde{N}_B\tilde{\psi}_{yB} + \sum_{i=1}^{\tilde{p}-1}\tilde{N}_{Ci}\Delta\tilde{\psi}_{yCi} \ , \tag{5.43}$$

where $\tilde{N}_A$, $\tilde{N}_B$ and $\tilde{N}_{Ci}$ are defined in Fig. 1.3, $\tilde{p}$ is the polynomial degree of $\tilde{\psi}_x$ and $\tilde{\psi}_y$ (the last term in eqns (5.42) and (5.43) will be missing if $\tilde{p}$ =1), then the proper choice for the deflection interpolation is

$$\tilde{w}_{A-C-B} = \tilde{N}_A\tilde{w}_A + \tilde{N}_B\tilde{w}_B + \sum_{i=1}^{\tilde{p}}\tilde{N}_{Ci}\Delta\tilde{w}_{Ci}. \tag{5.44}$$

The application of these functions for $\tilde{p} = 1$ and $\tilde{p} = 2$ along with 13 or 25 polynomial homogeneous solutions (5.35) leads to elements identical to Petrolito's quadrilaterals Q21-13 and Q32-25 [14].

5.3.4 Improved thick plate elements

We will now show that the performance of these successful elements can be further improved if $\tilde{w}$ is linked to $\tilde{\psi}_x$ and $\tilde{\psi}_y$ in agreement with the following consideration.

Since the stationary principle (5.61) [see Section 5.4] directly enforces equilibrium on generalized stresses $\tilde{\boldsymbol{\sigma}}$ corresponding to $\tilde{\mathbf{u}}$, it can be expected that element performance will be improved if some of the parameters of $\tilde{\mathbf{u}}$ are suitably linked so as to satisfy some static condition *a priori* (while preserving the necessary C^0 conformity). This may be accomplished if one observes that at the boundary of a rectangular element the polynomial degree of the shear force $\tilde{Q}_s$, obtained from moment equilibrium as

$$\tilde{Q}_s = \frac{\partial\tilde{M}_s}{\partial s} + \frac{\partial\tilde{M}_{ns}}{\partial n} \ , \tag{5.45}$$

where $M_s = M_{ij} s_i s_j$, is one degree lower (though the domain interpolation of $\tilde{\mathbf{u}}$, necessary for evaluation of the relation (5.45), is not given here explicitly, it is easy to see that for $\tilde{p} = 2$, for example, the rotation will be represented by a full quadratic polynomial plus the terms $x^2 y$ and xy^2 and the displacement will be a full cubic polynomial plus the terms $x^3 y$ and xy^3) than that derived from the tangential component of the shear deformation, namely

$$\tilde{Q}_s = C\left(\frac{\partial \tilde{w}}{\partial s} - \tilde{\psi}_s\right). \tag{5.46}$$

Thus, the term with the highest polynomial degree, $\tilde{p}$, in $\partial \tilde{w} / \partial s - \tilde{\psi}_s$ must be constrained to zero (for more details see e.g. [11]). This leads to the following relations

$$\Delta \tilde{w}_{C1} = \frac{1}{8}(\tilde{\psi}_{sB} - \tilde{\psi}_{sB}) l_{AB}, \tag{5.47}$$

for $\tilde{p} = 1$, and

$$\Delta \tilde{w}_{C\tilde{p}} = \frac{1}{2(1+\tilde{p})} \Delta\psi_{sC(\tilde{p}-1)} l_{AB}, \tag{5.48}$$

for $\tilde{p} > 1$, where l_{AB} is the length of side A-C-B and

$$\tilde{\psi}_s = \frac{1}{l_{AB}}(\tilde{\psi}_x \Delta x_{BA} + \tilde{\psi}_y \Delta y_{BA}), \tag{5.49}$$

where

$$\Delta x_{BA} = x_B - x_A, \quad \Delta y_{BA} = y_B - y_A. \tag{5.50}$$

Combining eqns (5.45)-(5.48) with eqn (5.42) finally yields

$$\tilde{w}_{A-C-B} = \tilde{N}_A \tilde{w}_A + \tilde{N}_B \tilde{w}_B + \frac{1}{8} \tilde{N}_{C1}[(\tilde{\psi}_{xB} - \tilde{\psi}_{xA})\Delta x_{BA} + (\tilde{\psi}_{yB} - \tilde{\psi}_{yA})\Delta y_{BA}], \tag{5.51}$$

for $\tilde{p} = 1$, and

$$\tilde{w}_{A-C-B} = \tilde{N}_A \tilde{w}_A + \tilde{N}_B \tilde{w}_B + \sum_{i=1}^{\tilde{p}-1} \tilde{N}_{Ci} \Delta \tilde{w}_{Ci} + \frac{1}{2(1+\tilde{p})} \tilde{N}_{C\tilde{p}}[\Delta\tilde{\psi}_{xC(\tilde{p}-1)} \Delta x_{BA} + \Delta\tilde{\psi}_{yC(\tilde{p}-1)} \Delta y_{BA}], \tag{5.52}$$

for $\tilde{p} > 1$. Thus, if eqn (5.44) is replaced by eqn (5.51) or (5.52), the polynomial degree of the $\tilde{w}$ interpolation is maintained ($p_{\tilde{w}} = \tilde{p} + 1$ as compared to $p_{\tilde{\psi}} = \tilde{p}$) while the number M of hierarchical parameters of each element side is reduced by one and is now equal to

$$M = 3(\tilde{p} - 1) \,. \tag{5.53}$$

It should be also noted that the above interpolation not only preserves the necessary C^0 conformity but also does not result in any strain when purely rigid body displacements and rotations are specified as nodal parameters.

With eqns (5.40)-(5.43), (5.51) and (5.52), the frame function $\tilde{\mathbf{u}} = \{\tilde{w}, \tilde{\psi}_x, \tilde{\psi}_y\}^T$ along a particular side of the element may be conveniently written in a matrix form as follows

$$\tilde{\mathbf{u}}_{A-C-B} = \tilde{\mathbf{N}}_A \mathbf{d}_A + \tilde{\mathbf{N}}_B \mathbf{d}_B \,, \tag{5.54}$$

for $\tilde{p} = 1$, where

$$\tilde{\mathbf{N}}_A = \begin{bmatrix} \tilde{N}_A & -\frac{1}{8}\tilde{N}_{C1}\Delta x_{BA} & -\frac{1}{8}\tilde{N}_{C1}\Delta y_{BA} \\ 0 & \tilde{N}_A & 0 \\ 0 & 0 & \tilde{N}_A \end{bmatrix}, \tag{5.55}$$

$$\tilde{\mathbf{N}}_B = \begin{bmatrix} \tilde{N}_B & \frac{1}{8}\tilde{N}_{C1}\Delta x_{BA} & \frac{1}{8}\tilde{N}_{C1}\Delta y_{BA} \\ 0 & \tilde{N}_B & 0 \\ 0 & 0 & \tilde{N}_B \end{bmatrix}, \tag{5.56}$$

and

$$\tilde{\mathbf{u}}_{A-C-B} = \tilde{\mathbf{N}}_A \mathbf{d}_A + \tilde{\mathbf{N}}_B \mathbf{d}_B + \tilde{\mathbf{N}}_C \mathbf{d}_C = \tilde{\mathbf{N}}_A \mathbf{d}_A + \tilde{\mathbf{N}}_B \mathbf{d}_B + \sum_{i=1}^{\tilde{p}-1} \tilde{N}_{Ci} \mathbf{d}_{Ci} \,, \tag{5.57}$$

for $\tilde{p} > 1$, where

$$\tilde{\mathbf{N}}_A = \tilde{N}_A \mathbf{I}, \quad \tilde{\mathbf{N}}_B = \tilde{N}_B \mathbf{I} \,, \tag{5.58}$$

with $\mathbf{I}$ is a 3×3 unit matrix, and

$$\tilde{\mathbf{N}}_{Ci} = \tilde{N}_{Ci} \mathbf{I} \,, \qquad (i = 1, 2, \cdots, \tilde{p} - 2, \text{ to be used only if } \tilde{p} > 2 \,), \tag{5.59}$$

$$\tilde{\mathbf{N}}_{C(\tilde{p}-1)} = \begin{bmatrix} \tilde{N}_{C(\tilde{p}-1)} & \dfrac{\Delta x_{BA}}{2(1+\tilde{p})}\tilde{N}_{C\tilde{p}} & \dfrac{\Delta y_{BA}}{2(1+\tilde{p})}\tilde{N}_{C\tilde{p}} \\ 0 & \tilde{N}_{C(\tilde{p}-1)} & 0 \\ 0 & 0 & \tilde{N}_{C(\tilde{p}-1)} \end{bmatrix}. \tag{5.60}$$

5.4 Variational formulation for HT thick plate elements

To develop the element stiffness equations, two variational functionals are introduced in this section. They are described as follows.

5.4.1 Variational functional $H(\mathbf{u},\tilde{\mathbf{u}})$

The variational principle corresponding to the functional $H(\mathbf{u},\tilde{\mathbf{u}})$ is stated as [7]

$$H(\mathbf{u},\tilde{\mathbf{u}}) = \Pi(\tilde{\mathbf{u}}) - \sum_e U^e(\boldsymbol{\varepsilon} - \tilde{\boldsymbol{\varepsilon}}) = \text{stationary}, \tag{5.61}$$

where $U^e(\varepsilon - \tilde{\varepsilon})$ is the strain energy of the difference $(\varepsilon - \tilde{\varepsilon}) = \mathbf{L}^T(\mathbf{u} - \tilde{\mathbf{u}})$ for element *e*, the sum $\sum_e$ is taken over all elements of the assembly, and $\Pi(\tilde{\mathbf{u}})$ is the total potential energy of the plate expressed in terms of the conforming displacements $\tilde{\mathbf{u}}$:

$$\Pi(\tilde{\mathbf{u}}) = \frac{1}{2}\int_\Omega \tilde{\boldsymbol{\varepsilon}}^T \mathbf{D}\boldsymbol{\varepsilon} d\Omega - \int_\Omega \tilde{\mathbf{u}}^T \bar{\mathbf{b}} d\Omega - \int_{\Gamma_\sigma} \tilde{\mathbf{v}}\bar{\mathbf{t}} ds\,, \tag{5.62}$$

where $\tilde{\mathbf{v}} = \{\tilde{w}, \tilde{\psi}_x, \tilde{\psi}_y\}^T$.

Performing vanishing variations with respect to $\mathbf{u}$ and $\tilde{\mathbf{u}}$ yields

$$\delta_{\mathbf{u}} H = 0 \Rightarrow \int_{\Omega_e} \delta\boldsymbol{\sigma}^T(\boldsymbol{\varepsilon} - \tilde{\boldsymbol{\varepsilon}}) d\Omega = \int_{\Gamma_e} \delta\mathbf{t}^T(\mathbf{v} - \tilde{\mathbf{v}}) ds = 0\,, \tag{5.63}$$

$$\delta_{\tilde{\mathbf{u}}} H = 0 \Rightarrow -\int_{\Gamma_\sigma} \delta\tilde{\mathbf{v}}^T \bar{\mathbf{t}} ds + \sum_e \int_{\Gamma_e} \delta\tilde{\mathbf{v}}^T \mathbf{t} ds = 0\,. \tag{5.64}$$

From eqns (5.63) and (5.64) it is easily seen that the stationary conditions associated with the statement (5.61) are simply

$$\mathbf{v} = \bar{\mathbf{v}}\,, \qquad (\text{on } \Gamma_u), \tag{5.65a}$$

$$\mathbf{t} = \bar{\mathbf{t}}\,, \qquad (\text{on } \Gamma_\sigma), \tag{5.65b}$$

$$\mathbf{v}_e = \mathbf{v}_f\,, \quad \mathbf{t}_e + \mathbf{t}_f = 0\,, \qquad (\text{on } \Gamma_e \cap \Gamma_f\,). \tag{5.65c}$$

Derivation of the element formulation is straightforward. Writing $\delta_{\tilde{\mathbf{u}}} H = 0$ in terms of contributions evaluated element by element,

$$\delta_{\tilde{\mathbf{u}}} H = \sum_e \delta_{\tilde{\mathbf{u}}} H_e\,, \tag{5.66}$$

assimilating $\delta_{\tilde{\mathbf{u}}} H_e$ to virtual work of equivalent nodal force $\mathbf{r}_e$ of the element

$$\delta_{\tilde{\mathbf{u}}} H_e = \delta \mathbf{d}_e^T \mathbf{r}_e\,, \tag{5.67}$$

and using eqns (5.63) and (5.64) leads to the standard force-displacement relationship

$$\mathbf{r}_e = \breve{\mathbf{r}}_e + \mathbf{k}_e \mathbf{d}_e\,, \tag{5.68}$$

where the load dependent part $\breve{\mathbf{r}}_e$ of $\mathbf{r}_e$ and the symmetric positive definite stiffness matrix $\mathbf{k}_e$ of the element are defined as

$$\breve{\mathbf{r}}_e = \mathbf{g} - \mathbf{S}\mathbf{H}^{-1}\mathbf{h} \quad \text{and} \quad \mathbf{k}_e = \mathbf{S}\mathbf{H}^{-1}\mathbf{S}^T\,. \tag{5.69}$$

Here, the auxiliary matrices **H**, **h**, **S** and **g** can be evaluated (see [7], for example) by performing the following boundary integrals

$$\mathbf{H} = \int_{\Gamma_e} \mathbf{T}^T \mathbf{N} ds = \int_{\Gamma_e} \mathbf{N}^T \mathbf{T} ds, \qquad \mathbf{S} = \int_{\Gamma_e} \tilde{\mathbf{N}}^T \mathbf{T} ds\,,$$

$$\mathbf{h} = \int_{\Gamma_e} \mathbf{T}^T \breve{\mathbf{u}} ds\,, \quad \mathbf{g} = \int_{\Gamma_e} \tilde{\mathbf{N}}^T \breve{\mathbf{t}} ds - \int_{\Gamma_{te}} \tilde{\mathbf{N}}^T \bar{\mathbf{t}} ds\,, \tag{5.70}$$

where $\mathbf{T} = \mathbf{A}\mathbf{D}\mathbf{L}^T\mathbf{N}$.

The important consequence of the fact that the integration is confined to the element boundary is that explicit knowledge of the domain interpolation of the auxiliary conforming field $\tilde{\mathbf{u}}$ is not necessary; it may be replaced by a suitable boundary interpolation of $\tilde{\mathbf{u}}$ (see Section 5.3).

Once the element assembly has been solved for nodal parameters, the undetermined parameters **c** of the internal field $\mathbf{u} = \breve{\mathbf{u}} + \mathbf{N}\mathbf{c}$ of any element can be evaluated in terms of its nodal parameters $\mathbf{d}_e$ as

$$\mathbf{c} = \mathbf{H}^{-1}(\mathbf{S}^T \mathbf{d}_e - \mathbf{h})\,. \tag{5.71}$$

5.4.2 Variational functional $\Pi_m(\mathbf{u}, \tilde{\mathbf{u}})$

An alternative variational functional presented in [17] for deriving hybrid-Trefftz thick plate elements is as follows:

$$\Pi_m = \sum_e \{\Pi_e + \int_{\Gamma_{e2}} (\overline{Q}_n - Q_n) w ds + \int_{\Gamma_{e4}} (\overline{M}_n - M_n)\psi_n ds$$
$$+ \int_{\Gamma_{e6}} (\overline{M}_{ns} - M_{ns})\psi_s ds - \int_{\Gamma_{e7}} (M_n \tilde{\psi}_n + M_{ns}\tilde{\psi}_s + Q_n \tilde{w}) ds\}, \tag{5.72}$$

where

$$\Pi_e = \int_{\Omega_e} U d\Omega - \int_{\Gamma_{e1}} Q_n \overline{w} ds - \int_{\Gamma_{e3}} M_n \overline{\psi}_n ds - \int_{\Gamma_{e5}} M_{ns} \overline{\psi}_s ds\ , \tag{5.73}$$

with

$$U = \frac{1}{2D(1-\mu^2)}[(M_{11}+M_{22})^2 + 2(1+\mu)(M_{12}^2 - M_{11}M_{22})] + \frac{1}{2C}(Q_x^2 + Q_y^2)\ , \tag{5.74}$$

and where eqn (5.5) is assumed to be satisfied, *a priori*. The boundary Γ_e of a particular element consists of the following parts:

$$\Gamma_e = \Gamma_{e1} + \Gamma_{e2} + \Gamma_{e7} = \Gamma_{e3} + \Gamma_{e4} + \Gamma_{e7} = \Gamma_{e5} + \Gamma_{e6} + \Gamma_{e7}\ , \tag{5.75}$$

where

$$\Gamma_{e1} = \Gamma_e \cap \Gamma_w,\ \Gamma_{e2} = \Gamma_e \cap \Gamma_Q,\ \Gamma_{e3} = \Gamma_e \cap \Gamma_{\psi_n},\ \Gamma_{e4} = \Gamma_e \cap \Gamma_{M_n},$$
$$\Gamma_{e5} = \Gamma_e \cap \Gamma_{\psi_s},\ \Gamma_{e6} = \Gamma_e \cap \Gamma_{M_{ns}}, \tag{5.76}$$

and Γ_{e7} is the inter-element boundary of the element.

Taking the vanishing variation of functional (5.72) yields

$$\delta\Pi_m = \int_{\Gamma_w} (w - \overline{w})\delta Q_n ds + \int_{\Gamma_{\psi n}} (\psi_n - \overline{\psi}_n)\delta M_n ds + \int_{\Gamma_{\psi s}} (\psi_s - \overline{\psi}_s)\delta M_{ns} ds$$
$$- \int_{\Gamma_R} (Q_n - \overline{Q}_n)\delta w ds - \int_{\Gamma_{M_n}} (M_n - \overline{M}_n)\delta\psi_n ds - \int_{\Gamma_{M_{ns}}} (M_{ns} - \overline{M}_{ns})\delta\psi_s ds$$
$$+ \sum_e \int_{\Gamma_{e7}} [(w - \tilde{w})\delta Q_n + (\psi_n - \tilde{\psi}_n)\delta M_n + (\psi_s - \tilde{\psi}_s)\delta M_{ns}$$
$$- Q_n \delta\tilde{w} - M_n \delta\tilde{\psi}_n - M_{ns}\delta\tilde{\psi}_s] ds = 0. \tag{5.77}$$

Hence, once again, the stationary condition of functional (5.72) leads to eqn (5.65) and the force-displacement relationship (5.68) may be derived from the functional in much the same manner as that described in Section 5.4.1.

5.5 Implementation of the new family of HT elements

The element will be designated according to the scheme

Qab-c/d, (5.78)

where (see Section 5.3) $\mathrm{a} = \tilde{p} + 1$ is the order of boundary approximation for $\tilde{w}$, $\mathrm{b} = \tilde{p}$ is the order of boundary approximation for $\tilde{\psi}_x$ and $\tilde{\psi}_y$, c is the number of functions in the polynomial set (5.35), and d is the number of functions in the set of modified Bessel functions (5.36).

A simplified designation,

$$\text{Qab-c rather than Qab-c/0,} \tag{5.79}$$

will be used if the set (5.36) is missing.

As before, the necessary (but not sufficient) condition for the resulting stiffness matrix $\mathbf{k}_e$ (see eqn (5.69)) to attain full rank may be stated as

$$m \geq k - r = k - 3, \tag{5.80}$$

where k and r are the numbers of nodal DOF of the element under consideration and of the discarded rigid body motion terms (r=3 for plate bending), m is the number of homogeneous solutions, $\mathbf{N}_i$, in the internal field (5.13). As was noted in Section 2.6, full rank can always be achieved by including more $\mathbf{N}_i$ functions in the internal field (5.13) although using the minimum number of m from eqn (5.80) does not always guarantee an element with full rank. In the present case, the situation is considerably complicated owing to the fact that the same m may be obtained by a large number of combinations of the numbers of functions taken from either of the independent sets (5.35) and (5.36). The Qab-c/d elements displayed in Table 5.2 are consistent with the scheme of alternating the functions in eqns (5.35) and (5.36), as shown in Table 5.1. They have been numerically tested and found to exhibit no rank deficiency and to perform better than other possible combinations of the functions in eqns (5.35) and (5.36). The Qab-c elements with purely polynomial functions (5.35) have also been considered. Though some of them (Q21-11 and Q43-33) exhibit one spurious zero energy mode, they may still be considered practically robust since this mode is not commutable in most practical situations (see Table 5.2) provided that the plate has at least minimal support (3 DOF blocked so as to prevent rigid body modes). Indeed, in such cases global singularity does not occur and such elements may be largely preferable to formally flawless (no spurious zero energy mode) but practically too rigid Q21-17 and Q43-41 elements.

In addition to the above, the following points must be noted when implementing the present family of elements:

(a) To prevent matrix **H** from being singular, polynomial set (5.33) does not include rigid body modes. As a consequence, the internal displacement field (5.13) will be in error by the rigid body components. If displacements inside the element are required, then the internal field (5.13) must be augmented with three rigid body modes (index r):

$$\mathbf{u}_r = \begin{bmatrix} 1 & x & y \\ 0 & 1 & 0 \\ 0 & 0 & 1 \end{bmatrix} \begin{Bmatrix} c_{1r} \\ c_{2r} \\ c_{3r} \end{Bmatrix}, \tag{5.81}$$

where c_{1r}, c_{2r} and c_{3r} are undetermined coefficients to be calculated by a simple procedure (see Section 4.6) used to make the augmented internal field match in a least-square sense the independent displacement frame $\tilde{\mathbf{u}}$ of the element. A simple but less accurate alternative (not used here) consists of calculating the displacements from the auxiliary field $\tilde{\mathbf{u}}$, which in the present case (C^0 conformity) may easily be defined over the element area rather than only at the boundary of the element.

(b) To ensure good numerical conditioning of matrix **H**, the local coordinates x and y originating at the element centre (Fig. 1.2) should be scaled, for example, by dividing them by the average distance between the origin and the element corners.

Table 5.2. Overview of new HT quadrilateral thick plate elements with either T-complete (polynomials+modified Bessel) or incomplete (purely polynomial) sets of Trefftz functions.

M	Number DOF	Condition (5.78)	Element	Actual m	Spurious modes	Min m for full rank
0	12	$m \geq 9$	Q21-9/1	10	0	-
			Q21-11	11	1Na	17
3	24	$m \geq 21$	Q32-17/5	22	0	-
			Q32-21	21	0	-
6	36	$m \geq 33$	Q43-25/9	34	0	-
			Q43-33	33	1Nb	41
9	48	$m \geq 45$	Q54-33/13	46	0	-
			Q54-45	45	0	-

Na — non-commutable in a mesh of 2 or more elements.
Nb — non-commutable with a minimum of 2×2 elements.

5.6 A 12 DOF quadrilateral element free of shear locking

This section describes a simple quadrilateral 12 DOF plate bending element, denoted by Q21-11, being robust and free of shear locking in the thinness limit. This element model was presented by Jirousek *et al.* [11] in 1995.

5.6.1 Basic relations

The governing equation (5.5) may conveniently be rewritten in an uncoupled form for w, ψ_x and ψ_y [20], namely

$$\nabla^4 w = \frac{\bar{q}}{D} - \frac{6}{5Gt}\nabla^2 \bar{q}\,, \tag{5.82}$$

$$\left(\frac{t^2}{10}\nabla^2 - 1\right)\left(\frac{\partial \overline{q}}{\partial x} - D\nabla^4\psi_x\right) = 0\,, \tag{5.83}$$

$$\left(\frac{t^2}{10}\nabla^2 - 1\right)\left(\frac{\partial \overline{q}}{\partial y} - D\nabla^4\psi_y\right) = 0\,, \tag{5.84}$$

where $\overline{m}_x = \overline{m}_y = 0$ has been assumed for simplicity.

The homogeneous part of the solution of (5.82) can be represented by biharmonic polynomials, which are given in eqn (5.33). Furthermore, Petrolito [14] has shown that the corresponding homogeneous solutions of eqns (5.83) and (5.84) may be obtained in the form

$$\psi_x = \frac{\partial w}{\partial x} + \frac{6D}{5Gt}\frac{\partial}{\partial x}\nabla^2 w\,, \tag{5.85}$$

$$\psi_y = \frac{\partial w}{\partial y} + \frac{6D}{5Gt}\frac{\partial}{\partial y}\nabla^2 w\,, \tag{5.86}$$

which in the thin plate limit, where $6D/5Gt \to 0$ if $h \to 0$, correctly models the constraint $\psi_x = \partial w/\partial x$, $\psi_y = \partial w/\partial y$.

As was pointed out in Section 5.3, a number of particular solutions of the Reissner-Mindlin theory may be found in [20]. In particular, for a uniform load $\overline{q}$, we have

$$\breve{\mathbf{u}} = \begin{Bmatrix} \breve{w} \\ \breve{\psi}_x \\ \breve{\psi}_y \end{Bmatrix} = \begin{Bmatrix} \dfrac{\overline{q}}{64D}\left(r^2 - \dfrac{96D}{5Gt}\right) \\ \dfrac{xr^2\overline{q}}{16D} \\ \dfrac{yr^2\overline{q}}{16D} \end{Bmatrix}. \tag{5.87}$$

5.6.2 Assumed field

5.6.2.1 Conforming field $\tilde{\mathbf{u}} = \tilde{\mathbf{N}}\mathbf{d}$ The crucial point of the formulation is the choice of the C^0 conforming field $\tilde{\mathbf{u}} = \{\tilde{w}, \tilde{\psi}_x \tilde{\psi}_y\}^T$. Since in the thin plate limit $\psi_x = \partial w/\partial x$ and $\psi_y = \partial w/\partial y$, the order of the polynomial interpolation of the displacement has to be one degree higher than that of the rotations if the resulting element is to be free of shear locking. Hence, if (Fig. 5.1)

$$\tilde{\psi}_x = \sum_{i=1}^{4} \tilde{N}_i \tilde{\psi}_{xi} \quad \text{and} \quad \tilde{\psi}_y = \sum_{i=1}^{4} \tilde{N}_i \tilde{\psi}_{yi}\,, \tag{5.88}$$

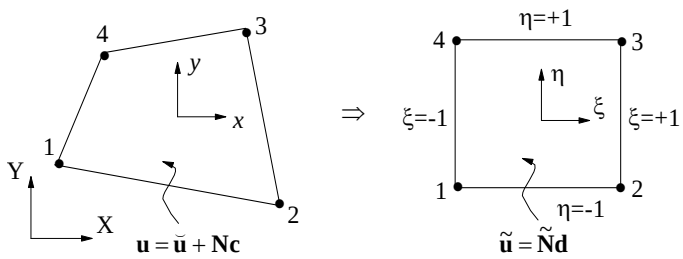

Fig. 5.1: Typical HT 4-node element with definition of ξ and η.

where

$$\tilde{N}_j = \tfrac{1}{4}(1+\xi_j\xi)(1+\eta_j\eta)\,, \tag{5.89}$$

with ξ_j and η_j being the values of ξ and η at node j (see Fig. 5.1), then the proper choice for the displacement field interpolation is

$$\tilde{w} = \sum_{i=1}^{4} \tilde{N}_i w_i + \sum_{i=1}^{4} \tilde{N}_{ik} \Delta w_{ik}\,, \tag{5.90}$$

where

$$k = i+1 \;\text{ if } i<4 \;\text{ and }\; k=1 \;\text{ if } i=4\,, \tag{5.91}$$

$$\begin{aligned} \tilde{N}_{12} &= \frac{1}{2}(1-\xi^2)(1-\eta), \quad \tilde{N}_{23} = \frac{1}{2}(1-\eta^2)(1+\xi), \\ \tilde{N}_{34} &= \frac{1}{2}(1-\xi^2)(1+\eta), \quad \tilde{N}_{41} = \frac{1}{2}(1-\eta^2)(1-\xi). \end{aligned} \tag{5.92}$$

5.6.2.2 Trefftz field $\mathbf{u} = \breve{\mathbf{u}} + \mathbf{Nc}$ It has been noted that, in the HT FE approach, the proper choice of the number *m* of the homogeneous solution in eqn (5.13) is of great importance to the element performance and to the stability of the solution. In our case, with the number of DOF=12, the rank condition (5.80) yields *m*≥9. However, since eqn (5.80) is only a necessary but not a sufficient condition, using the minimal number of Trefftz terms does not always guarantee an element with full rank. In our case the use of *m*=9 results in one spurious zero-energy mode if the element is rectangular (no such mode appears for a non-rectangular element). Since full rank can always be achieved by including more

Trefftz terms in eqn (5.13), the standard eigenvalue control of the stiffness matrix continues, while incrementing *m* by steps of two until *m*=17, which has been found to stabilize the element. However, the use of such a large *m* involves an important computational penalty due to the size of matrix **H** in eqn (5.70), which must be formed and then numerically inverted. Therefore, in order to avoid such an expensive calculation, close attention has been paid to the spurious zero-energy mode encountered for lower values of *m*. It is evident that the use of *m*=9, 11, 13 and 15 invariably results in a single extra zero-energy mode, which involves the rotational components only, while the deflections remain zero. It has been found that this mode is non-commutable in a mesh of two or more elements and, provided that the structure has at least a minimal support (3 DOF blocked), a global singularity does not occur. As a consequence, any *m* from 9 to15 yields an element which is robust under all practical conditions. The element has finally been implemented with *m*=11, a value selected as the best compromise between accuracy and computational effort.

The explicit form of the corresponding 3×11 matrix **N**, involving the 11 homogeneous solution derived by the application of the relations (5.33), (5.85) and (5.86) is given as follows:

$$\mathbf{N} = \begin{bmatrix} \mathbf{N}_1 & \mathbf{N}_2 & \mathbf{N}_3 \end{bmatrix}, \tag{5.93}$$

where

$$\mathbf{N}_1 = \begin{bmatrix} x^2+y^2 & x^2-y^2 & 2xy \\ 2x & 2x & 2y \\ 2y & -2y & 2x \end{bmatrix}, \tag{5.94}$$

$$\mathbf{N}_2 = \begin{bmatrix} x(x^2+y^2) & y(x^2+y^2) & x(x^2-3y^2) & y(3x^2-y^2) \\ 3x^2+y^2+8C & 2xy & 3(x^2-y^2) & 6xy \\ 2xy & x^2+3y^2+8C & -6xy & 3(x^2-y^2) \end{bmatrix}, \tag{5.95}$$

$$\mathbf{N}_3 = \begin{bmatrix} x^4-y^4 & 2xy(x^2+y^2) & x^4-6x^2y^2+y^4 & 4xy(x^2-y^2) \\ -x(4x^2+24C) & 2y(3x^2+y^2)+24Cy & 4x(x^2-3y^2) & 4y(3x^2-y^2) \\ -y(4y^2+24C) & 2x(x^2+3y^2)+24Cx & 4y(y^2-3x^2) & 4x(x^2-3y^2) \end{bmatrix}. \tag{5.96}$$

5.7 Extension to thick plates on an elastic foundation

5.7.1 T-complete functions and particular solution

As in Section 4.9, in the case of a thick plate resting on an elastic foundation the left-hand side of eqn (5.17) and the boundary equation (5.7) must be augmented by the terms Kw and $-\alpha G_p w$, respectively:

$$C\left(\nabla^2 w - \frac{\partial \psi_x}{\partial x} - \frac{\partial \psi_y}{\partial y}\right) + Kw = \overline{q}\ , \quad \text{(in } \Omega\text{)}, \tag{5.97}$$

$$M_n = M_{ij} n_i n_j - \alpha G_p w = \overline{M}_n\ , \qquad \text{(on } \Gamma_{Mn}\text{)}, \tag{5.98}$$

where α and K are defined in Section 4.9.

Following the method in Section 5.3, the transverse deflection w and the rotations ψ_x, ψ_y may be expressed in terms of two auxiliary functions, g and f, by eqns (5.29) and (5.19). The function f is again obtained as a solution of the modified Bessel equation (5.31), while for g, instead of the biharmonic equation (5.30), the following differential equation now applies [17]:

$$D\nabla^4 g + \frac{K}{C}\nabla^2 g - Kg = \overline{q}\ . \tag{5.99}$$

The corresponding T-complete system of homogeneous solutions is obtained in a manner similar to that in Section 4.9, as

$$g(r,\theta) = c_1 G_0(r) + \sum_{j=1}^{\infty}[c_{2j} G_j(r)\cos j\theta + c_{2j+1} G_j(r)\sin j\theta]\ , \tag{5.100}$$

where

$$G_j(r) = I_j(r\sqrt{C_2}) - J_j(r\sqrt{C_1})\ , \tag{5.101}$$

with

$$C_1 = \sqrt{(\frac{k_w}{2C})^2 + \frac{k_w}{D}} + \frac{k_w}{2C}\ , \qquad C_2 = \sqrt{(\frac{k_w}{2C})^2 + \frac{k_w}{D}} - \frac{k_w}{2C}\ , \tag{5.102}$$

for a Winkler-type foundation and

$$C_1 = \frac{\sqrt{b} + k_P / C + G_P / D}{2(1 - G_P / C)}, \qquad C_2 = \frac{\sqrt{b} - k_P / C - G_P / D}{2(1 - G_P / C)},$$

$$b = \left(\frac{k_P}{C} + \frac{G_P}{D}\right)^2 + \frac{4k_P}{D}(1 - \frac{G_P}{C})\ , \tag{5.103}$$

for a Pasternak-type foundation.

With solution (5.100), the related internal function $\mathbf{N}_j$ in eqn (5.13) can be determined. As a consequence, its generalized boundary forces and displacements are derived from eqns (5.7)-(5.13) and (5.42)-(5.44), and we denote

$$\mathbf{t} = \begin{Bmatrix} Q_n \\ M_n \\ M_{ns} \end{Bmatrix} = \mathbf{A}_1 \overline{\mathbf{D}} \mathbf{L}_1 \mathbf{u} - \begin{Bmatrix} 0 \\ \alpha w \\ 0 \end{Bmatrix} = \begin{Bmatrix} \breve{Q}_n \\ \breve{M}_n \\ \breve{M}_{ns} \end{Bmatrix} + \begin{Bmatrix} \mathbf{P}_{11} \\ \mathbf{P}_{12} \\ \mathbf{P}_{13} \end{Bmatrix} \mathbf{c} = \breve{\mathbf{t}} + \mathbf{P}_1 \mathbf{c}\,, \tag{5.104}$$

$$\mathbf{v} = \begin{Bmatrix} w \\ \psi_n \\ \psi_s \end{Bmatrix} = \begin{Bmatrix} \breve{w} \\ \breve{\psi}_n \\ \breve{\psi}_s \end{Bmatrix} + \begin{Bmatrix} \mathbf{P}_{21} \\ \mathbf{P}_{22} \\ \mathbf{P}_{23} \end{Bmatrix} \mathbf{c} = \breve{\mathbf{v}} + \mathbf{P}_2 \mathbf{c}\,, \tag{5.105}$$

$$\tilde{\mathbf{v}} = \begin{Bmatrix} \tilde{w} \\ \tilde{\psi}_n \\ \tilde{\psi}_s \end{Bmatrix} = \begin{Bmatrix} \mathbf{P}_{31} \\ \mathbf{P}_{32} \\ \mathbf{P}_{33} \end{Bmatrix} \mathbf{d} = \mathbf{P}_3 \mathbf{d}\,, \tag{5.106}$$

where

$$\mathbf{A}_1 = \begin{bmatrix} n_x & n_y & 0 & 0 & 0 \\ 0 & 0 & n_x^2 & n_y^2 & 2n_x n_y \\ 0 & 0 & -n_x n_y & n_x n_y & n_x^2 - n_y^2 \end{bmatrix},$$

$$\overline{\mathbf{D}} = \begin{bmatrix} \mathbf{D}_1 & 0 \\ 0 & \mathbf{D}_2 \end{bmatrix}, \quad \mathbf{D}_1 = \begin{bmatrix} C & 0 \\ 0 & C \end{bmatrix}, \quad \mathbf{D}_2 = \frac{D}{2} \begin{bmatrix} 2 & 2\mu & 0 \\ 2\mu & 2 & 0 \\ 0 & 0 & 1-\mu \end{bmatrix},$$

$$\mathbf{L}_1 = \begin{bmatrix} \partial/\partial x & \partial/\partial y & 0 & 0 & 0 \\ -1 & 0 & -\partial/\partial x & 0 & -\partial/\partial y \\ 0 & -1 & 0 & -\partial/\partial y & -\partial/\partial x \end{bmatrix}^T. \tag{5.107}$$

The particular solution $\breve{g}$ in eqn (5.37) is obtained by integrating its Green's function. The Green's function $g^*(r_{PQ})$ for eqn (5.99) has been given in [16] as

$$g^*(r_{PQ}) = \frac{1}{D(C_1 + C_2)} \left[\frac{1}{2\pi} K_0(r_{PQ}\sqrt{C_2}) - \frac{1}{4} Y_0(r_{PQ}\sqrt{C_1}) \right], \tag{5.108}$$

where r_{PQ} is defined as in Section 2.4, $Y_0(\,)$ and $K_0(\,)$ are, respectively, the Bessel and modified Bessel functions of second kind with zero order. This makes

it possible to evaluate $\breve{g}$ due a load $\overline{q}$ as

$$\breve{g}(P) = \int_{\Omega_e} \overline{q}(Q) g^*(r_{PQ}) d\Omega(Q) , \tag{5.109}$$

where Q represents the source point and P is the point under consideration.

5.7.2 Variational formulation

The variational functional used to derive HT FE formulation for thick plates on an elastic foundation is the same as eqn (5.72) except that the strain energy function U in eqn (5.74) is now replaced by U^*:

$$U^* = U + V^* , \tag{5.110}$$

in which U and V^* are defined in eqns (5.74) and (4.110) respectively. By way of the properties of the internal trial functions, the expression (5.72) for the present case can be further simplified as

$$\begin{aligned}\Pi_m = \sum_e \Bigg\{ & \frac{1}{2}\int_{\Omega_e} \overline{q} w d\Omega - \int_{\Gamma_{e1}} Q_n \overline{w} ds - \int_{\Gamma_{e3}} M_n \overline{\psi}_n ds - \int_{\Gamma_{e5}} M_{ns} \overline{\psi}_s ds \\ & + \int_{\Gamma_{e2}} (\overline{Q}_n - Q_n) w ds + \int_{\Gamma_{e4}} (\overline{M}_n - M_n) \psi_n ds + \int_{\Gamma_{e6}} (\overline{M}_{ns} - M_{ns}) \psi_s ds \\ & + \frac{1}{2}\int_{\Gamma_e} (M_n \psi_n + M_{ns} \psi_s + Q_n w) ds - \int_{\Gamma_{e7}} (M_n \tilde{\psi}_n + M_{ns} \tilde{\psi}_s + Q_n \tilde{w}) ds \Bigg\}.\end{aligned} \tag{5.111}$$

The vanishing variation of this formulation leads straightforwardly to the standard force-displacement relationship [17]

$$\mathbf{Kd} = \mathbf{P} , \tag{5.112}$$

where

$$\mathbf{K} = \mathbf{SH}^{-1}\mathbf{S}^T , \qquad \mathbf{P} = \mathbf{SH}^{-1}\mathbf{r}_1 + \mathbf{r}_2 , \tag{5.113}$$

with

$$\mathbf{H} = -\int_{\Gamma_e} \mathbf{P}_1^{\mathrm{T}} \mathbf{P}_2 ds + 2\int_{\Gamma_{e2}} \mathbf{P}_{11}^{\mathrm{T}} \mathbf{P}_{21} ds + +2\int_{\Gamma_{e4}} \mathbf{P}_{12}^{\mathrm{T}} \mathbf{P}_{22} ds + 2\int_{\Gamma_{e6}} \mathbf{P}_{13}^{\mathrm{T}} \mathbf{P}_{23} ds , \tag{5.114}$$

$$\mathbf{S} = -\int_{\Gamma_{1e}} \mathbf{P}_3^{\mathrm{T}} \mathbf{P}_1 ds , \tag{5.115}$$

$$\mathbf{r}_2 = -\int_{\Gamma_{e7}} \mathbf{P}_3^{\mathrm{T}} \breve{\mathbf{t}} ds , \tag{5.116}$$

$$\mathbf{r}_1 = \frac{1}{2}\int_{\Omega_e} (\mathbf{N}^T)_1 \bar{q} d\Omega - \int_{\Gamma_{e1}} \mathbf{P}_{11}^{\mathrm{T}} \bar{w} ds - \int_{\Gamma_{e3}} \mathbf{P}_{12}^{\mathrm{T}} \bar{\psi}_n ds - \int_{\Gamma_{e5}} \mathbf{P}_{13}^{\mathrm{T}} \bar{\psi}_s ds$$

$$+ \frac{1}{2}\int_{\Gamma_e} (\mathbf{P}_1^{\mathrm{T}} \breve{\mathbf{u}} + \mathbf{P}_2^T \breve{\mathbf{t}}) ds - \int_{\Gamma_{e2}} [\mathbf{P}_{11}^{\mathrm{T}} \breve{w} + \mathbf{P}_{21}^T (\breve{Q}_n - \bar{Q}_n)] ds$$

$$- \int_{\Gamma_{e4}} [\mathbf{P}_{12}^{\mathrm{T}} \breve{\psi}_n + \mathbf{P}_{22}^T (\breve{M}_n - \bar{M}_n)] ds - \int_{\Gamma_{e6}} [\mathbf{P}_{13}^{\mathrm{T}} \breve{\psi}_s + \mathbf{P}_{23}^T (\breve{M}_{ns} - \bar{M}_{ns})] ds \,, \quad (5.117)$$

where $(\mathbf{N})_1$ represents the first column of the matrix **N**.

5.8 Sensitivity to mesh distortion

This study is based on the comparison of percentage errors for uniform and distorted 4×4 meshes (see Fig. 4.8) over the whole uniformly loaded square plate with hard-simple support. Both thick (L/t=10) and very thin (L/t=1000) plates are considered, and their results have been displayed in Tables 5.3 and 5.4. As expected, this study again confirms that the results are not overly sensitive to mesh distortion.

Table 5.3. % errors for uniform and distorted 4×4 mesh (Fig.4.8). Uniformly loaded simply supported (SS2) thick square plate (L/t=10).

M	Element Type	Δw_c% Uniform mesh	Δw_c% Distorted mesh d=L/8	Δw_c% Distorted mesh d=L/4	ΔM_{xc}% Uniform mesh	ΔM_{xc}% Distorted mesh d=L/8	ΔM_{xc}% Distorted mesh d=L/4
0	Q21-11	0.20	–0.13	–1.06	0.26	2.58	5.53
	Q21-9/1	0.21	–0.11	–0.97	0.21	–2.42	3.34
3	Q32-21	–0.01	–0.01	–0.01	–0.04	0.05	0.25
	Q32-17/5	–0.01	–0.01	–0.02	0.12	0.02	0.08
6	Q43-33	0.00	0.00	0.00	0.00	0.00	–0.01
	Q43-25/9	0.00	0.00	0.00	0.01	0.00	–0.03
Exact		$w_c = 0.0042728\bar{q}L^4/D$			$M_{xc} = 0.0478864\bar{q}L^2$		

5.9 Numerical assessment

5.9.1 Preliminary remarks

Unlike classical thin plate theory, Reissner-Mindlin theory requires three independent boundary conditions to be prescribed at the boundary of the plate, namely:

(a) $w = M_n = M_{ns} = 0$ …soft simple support (SS1);

(b) $w = M_n = \psi_s = 0$ …hard simple support (SS2);

(c) $w = \psi_n = \psi_s = 0$ …clamped edge (C);

(d) $Q_n = M_n = M_{ns} = 0$ …free edge (F).

Table 5.4. % errors for uniform and distorted 4×4 mesh (Fig. 4.8). Uniformly loaded simply supported (SS2) thin square plate (L/t=1000).

M	Element Type	Δw_c% Uniform mesh	Δw_c% Distorted mesh $d=L/8$	Δw_c% Distorted mesh $d=L/4$	ΔM_{xc}% Uniform mesh	ΔM_{xc}% Distorted mesh $d=L/8$	ΔM_{xc}% Distorted mesh $d=L/4$
0	Q21-11	–0.14	–0.65	–2.10	–0.09	1.78	3.00
3	Q32-21	–0.01	–0.01	–0.02	0.03	0.05	–0.09
6	Q43-33	0.00	0.00	0.00	–0.01	0.00	0.01
9	Q54-45	0.00	0.00	0.00	0.00	0.00	0.01
Exact		$w_c = 0.00406237\bar{q}L^4 / D$			$M_{xc} = 0.0478864\bar{q}L^2$		

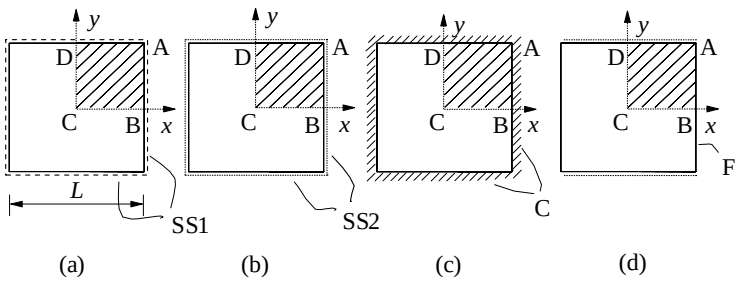

Fig. 5.2: Benchmark examples of square plates with various boundary conditions. Hatched area: discretized symmetric plate quadrant.

Most of the numerical studies presented in this section refer to the conventionally used square plate test (Fig. 5.2). The information about mesh density concerns a symmetric quadrant of the plate. Furthermore, a Poisson ratio of $\mu = 0.3$ has been used in all examples and the displacement results are the frame values ($w = \tilde{w}$).

The converged reference results of the thick plate theory (results designated as ‘exact’ in the following studies) have been generated:

(a) by application of the method outlined for soft simple support (SS1) in [13];

(b) by the series solution presented for hard simple support (SS2) in [20];

(c) by application of the methods outlined for clamped edge (C) and for the combination of free (F) and simply supported (SS2) boundaries (Fig. 5.2(d)) in [13].

5.9.2 Uniformly loaded square plate with hard simple support (SS2)

The aim of this study is to investigate the performance of the Qab-c elements from Table 5.5. The results for central displacement and bending moment for a thick plate (L/t=10), a thin plate(L/t=100) and a very thin plate (L/t=1000) are given in Table 5.5. It can be seen that both the *h*- and the *p*-extensions perform very nicely and that no shear locking appears for the thinnest plate with L/t=1000. In this case the thick plate theory approximates well the classical thin plate solution,

$$w_c = 0.00406237\bar{q}L^4 / D\,, \qquad M_{xc} = 0.0478864\bar{q}L^2\,,$$

obtained from the converged double series Navier solution [20].

Table 5.5. *h*- and *p*-convergence study for central deflection and moment for simply supported (SS2) square plate (Fig. 5.2b) solved with Qab-c type of thick plate elements.

Mesh	M	$10^2 Dw_c : \bar{q}L^4$			$10M_{11c} : \bar{q}L^2$		
		L/t =10	100	1000	L/t =10	100	1000
1×1	0	0.418754	0.390909	0.390628	0.487982	0.474130	0.473960
	3	0.426476	0.405531	0.405318	0.482045	0.489321	0.489545
	6	0.427448	0.406596	0.406388	0.479180	0.478509	0.478492
	9	0.427284	0.406440	0.406231	0.478895	0.478811	0.478796
2×2	0	0.428157	0.405878	0.405650	0.480086	0.478462	0.478419
	3	0.427241	0.406410	0.406202	0.478658	0.479022	0.479029
	6	0.427288	0.406447	0.406239	0.478870	0.478830	0.478832
	9	0.427284	0.406446	0.406237	0.478864	0.478865	0.478865
4×4	0	0.427644	0.406510	0.406296	0.479043	0.478868	0.478856
	3	0.427282	0.406444	0.406236	0.478835	0.478877	0.478879
	6	0.427284	0.406446	0.406237	0.478866	0.478861	0.478861
	9				0.478864	0.478864	0.478864
Exact		0.427284	0.406446	0.406237	0.478864	0.478864	0.478864

5.9.3 Uniformly loaded square plate with soft simple support (SS1)

5.9.3.1 Imposing the SS1 boundary conditions in FE calculation The difficulty of accurately imposing the SS1 boundary conditions ($w = M_n = M_{ns} = 0$) is attributable to the fact that the conditions $M_n = M_{ns} = 0$ allow fully unconstrained rotations $\tilde{\psi}_x$ and $\tilde{\psi}_y$, but imposing to zero of the displacement parameters alone

$$\tilde{w}_A = \tilde{w}_B = 0\,, \quad \text{(in eqn (5.51))}, \tag{5.118}$$

or

$$\tilde{w}_A = \tilde{w}_B = \Delta\tilde{w}_{C1} = \cdots = \Delta\tilde{w}_{C(\tilde{p}-1)} = 0\,, \quad \text{(in eqn (5.52))}, \tag{5.119}$$

is not sufficient for $\tilde{w}$ along the side A-C-B to vanish. Following [26], the simple device of setting

$$\tilde{N}_{C1} = 0\,, \qquad \text{(in eqn (5.51))}, \tag{5.120}$$

and similarly, in our case, of setting

$$\tilde{N}_{C\tilde{p}} = 0\,, \qquad \text{(in eqn (5.52))}, \tag{5.121}$$

removes the link between $\tilde{w}$ and $\tilde{\psi}_s = (\tilde{\psi}_x \Delta x_{BA} + \tilde{\psi}_y \Delta y_{BA})/l_{AB}$ and yields vanishing of $\tilde{w}$ along the whole side A-C-B.

Table 5.6. Uniformly loaded simply supported (SS1) square plate (Fig. 5.2a). A 4×4 mesh of Q32-17/5 elements over a symmetric quadrant (*L*/*t*=10).

Method of imposing	No linking $\tilde{N}_{C\tilde{p}} = 0$	Last DOF $\tilde{\psi}_s$ left free	Last DOF $\tilde{\psi}_s$ blocked
$\frac{10^3 D w_c}{\bar{q} L^4}$	4.6211	4.6233	4.6098
Δw_c%	0.09	0.14	–0.15
$\frac{10^2 M_{xc}}{\bar{q} L^2}$	5.0997	5.1010	5.0903
ΔM_{xc}%	0.08	0.11	–0.11
$\frac{10 Q_{xB}}{\bar{q} L}$	–3.9511	–3.9037	–4.0709
ΔQ_{xB}%	–6.25	–7.37	–3.40

The price paid for this facility is, however, a non-standard FE coding, since eqns (5.120) and (5.121) have to be imposed at the element level, in the element subroutine. In the case of the Q21-11 element (*M*=0), which was studied in [11], it has been shown that condition (5.118) alone still leads to excellent results and allows a fast convergence to the exact solution. Similarly, for higher-order elements (*M* >0), condition (5.121) may be neglected and the SS1 condition approached, without a significant loss of accuracy (see Table 5.6), in either of the following two ways:

(a) let rotation be completely unconstrained and, as a consequence, tolerate in eqns (5.51) and (5.52) a small parasitic displacement

$$\frac{1}{2(1+\tilde{p})}\tilde{N}_{C\tilde{p}}(\Delta\tilde{\psi}_{xC(\tilde{p}-1)}\Delta x_{BA}+\Delta\tilde{\psi}_{yC(\tilde{p}-1)}\Delta y_{BA})=\frac{1}{2(1+\tilde{p})}\tilde{N}_{C\tilde{p}}\Delta\tilde{\psi}_{sC(\tilde{p}-1)}l_{BA}, \quad (5.122)$$

where $\Delta\psi_{sC(\tilde{p}-1)}$ is the last parameter of tangent rotation $\tilde{\psi}_s$.

(b) in order to cancel the above parasitic displacement and to obtain $\tilde{w}$ along A-C-B, accept a partial constraint on $\tilde{\psi}_s$,

$$\Delta\psi_{sC(\tilde{p}-1)}=0. \quad (5.123)$$

Though the difference in accuracy is generally small (see Table 5.6), this method has a small advantage over method (a) and therefore is applied in numerical studies presented in the following section.

Table 5.7. Uniformly loaded simply supported (SS1) square plate (*L/t*=10). Comparison of solutions with incomplete (Qab-c) and T-complete (Qab-c/d) Trefftz function sets.

Quantity	Mesh	*M*=0		*M*=3		*M*=6		*M*=9		Exact
		Q21-11	Q21-9/1	Q32-21	Q32-17/5	Q43-33	Q43-25/9	Q54-45	Q54-33/13	
$\frac{10^3 Dw_c}{\bar{q}L^4}$	1×1	5.6689	4.6282	4.6223	4.5821	6.7896	4.7534	6.8876	4.6437	4.6169
	2×2	4.7122	4.5591	4.7235	4.5988	5.4271	4.6196	5.4643	4.6167	
	4×4	4.6184	4.5738	4.7133	4.6099	4.9563	4.6167	4.9854	4.6169	
	8×8	4.6183	4.5992	4.6602	4.6158	4.7403	4.6169	4.7652	4.6169	
$\frac{10^2 M_{xc}}{\bar{q}L^2}$	1×1	7.2608	5.6160	4.9597	5.0277	6.5187	5.2415	6.4949	5.4652	5.0957
	2×2	4.8964	5.0626	5.2246	5.1272	5.8126	5.0845	5.8454	5.1004	
	4×4	5.0834	5.0584	5.1839	5.0896	5.3998	5.0955	5.4259	5.0957	
	8×8	5.0878	5.0794	5.1348	5.0948	5.2062	5.0957	5.2281	5.0957	
$-\frac{10Q_{xB}}{\bar{q}L}$	1×1	3.9991	2.8822	1.7602	0.9604	0.9935	4.6230	2.3509	6.0395	4.2143
	2×2	3.4341	2.6470	2.6945	3.1521	3.0343	4.5525	2.7226	4.1887	
	4×4	3.6095	3.8885	3.7539	4.0659	3.4586	4.2213	2.6380	4.2132	
	8×8	3.7295	4.1046	4.1186	4.2042	3.9417	4.2116	2.6246	4.2182	

5.9.3.2 Comparison of solutions with *p*-elements based on incomplete and T-complete sets of Trefftz functions The HT element results displayed for *L/t*=10 in Table 5.7 and the percentage errors shown for *L/t*=10 and *L/t*=40 in Tables 5.8 and 5.9 lead to the following conclusions:

(a) The *p*-extension based on the Qab-c elements diverges. Therefore, if only the polynomial set of Trefftz functions is available, the best choice is the *h*-extension based on the Q21-11 lowest order element.

(b) Both the *h*- and *p*-extensions rapidly converge toward the exact results if use is made of the Qab-c/d elements. Nevertheless, the necessary condition for the

Table 5.8. Uniformly loaded simply supported (SS1) square plate (L/t=10). percent errors of solutions with incomplete (Qab-c) and T-complete (Qab-c/d) Trefftz function sets.

Quantity	Mesh	M=0		M=3		M=6		M=9	
		Q21-11	Q21-9/1	Q32-21	Q32-17/5	Q43-33	Q43-25/9	Q54-45	Q54-33/13
Δw_c%	1×1	22.79	0.24	0.15	–0.75	47.06	2.96	49.18	0.58
	2×2	2.06	–1.25	2.31	–0.39	17.55	0.06	18.35	0.00
	4×4	0.03	–0.93	2.09	–0.15	7.35	0.00	7.98	0.00
	8×8	0.03	–0.38	0.94	–0.02	2.67	0.00	3.21	
ΔM_{xc}%	1×1	42.49	10.21	–2.67	–1.33	27.93	2.86	27.46	7.25
	2×2	–3.91	–0.65	2.53	0.62	14.07	–0.22	14.72	0.09
	4×4	–0.24	–0.73	1.73	–0.12	5.97	0.00	6.48	0.00
	8×8	–0.16	–0.32	0.77	–0.02	2.17	0.00	2.60	0.00
ΔQ_{xB}%	1×1	–5.11	–31.61	–58.23	–122.79	–76.43	9.70	–44.22	43.31
	2×2	–18.51	–37.19	–36.06	–25.21	–28.00	8.02	–35.40	–0.61
	4×4	–14.35	–7.73	–10.92	–3.52	–17.93	0.17	–37.40	–0.03
	8×8	–7.95	–2.60	–2.27	–0.24	–6.47	–0.07	–37.72	0.09

Table 5.9. Uniformly loaded simply supported (SS1) square plate (L/t=40). percent errors of solutions with incomplete (Qab-c) and T-complete (Qab-c/d) Trefftz function sets

Quantity	Mesh	M=0		M=3		M=6		M=9	
		Q21-11	Q21-9/1	Q32-21	Q32-17/5	Q43-33	Q43-25/9	Q54-45	Q54-33/13
Δw_c%	1×1	27.49	27.49	3.40	3.02	57.12	53.21	60.15	35.17
	2×2	5.01	4.44	2.97	2.39	21.62	11.13	21.85	1.87
	4×4	1.14	0.66	1.74	0.57	9.07	0.50	9.16	0.01
	8×8	0.05	–0.32	1.12	–0.02	4.14	0.01	4.24	0.00
ΔM_{xc}%	1×1	48.88	48.88	–1.42	8.42	35.09	37.21	35.56	–59.79
	2×2	–1.22	–0.28	2.85	1.14	12.26	7.79	16.46	2.20
	4×4	0.65	0.33	1.37	0.45	6.88	0.38	6.94	0.01
	8×8	0.01	–0.27	0.86	–0.02	3.15	0.01	3.22	0.00
ΔQ_{xB}%	1×1	–4.09	–4.09	–76.76	–171.66	–75.88	–232.40	–111.83	–166.95
	2×2	–16.86	–42.52	–61.19	–136.14	–15.50	282.60	–92.04	277.89
	4×4	–42.04	–80.65	–50.10	–98.46	–24.95	67.32	–57.43	21.04
	8×8	–10.79	–40.00	–29.85	–22.50	–24.81	8.02	–35.01	–0.69

p-extension to converge is a certain minimal density of the HT element mesh (e.g. 2×2 for L/t=10 and 4×4 for L/t=40).

The above minimal density requirement is easy to understand. Clearly, the boundary layer effect [10] and the much simpler low gradient behavior further away from the boundary cannot be accurately represented within a single band of elements adjacent to the plate edge. Furthermore, the width of the boundary layer decreases with decreasing L/t ratio of the plate.

5.9.4 Uniformly loaded square plate with clamped edges (Fig. 5.2c)

The results for *L/t*=10 and the percentage errors for *L/t*=10 and *L/t*=40 are displayed in Tables 5.10-5.12. As expected, both *h*- and *p*-extension processes based on the Qab-c/d elements with T-complete solution functions rapidly converge to the exact solution. In contrast, the Qab-c elements behave quite differently. While the *h*-extension again converges toward the exact results, this convergence is now slower than that of the Qab-c/d elements. In the Qab-c case the mesh density, limited in Table 5.10 to 8×8 elements, had to be extended to 64×64 elements in order to confirm this statement. However, what is most interesting is the fact that for any fixed mesh density the *p*-extension now yields a different converged value. Though for practical purposes this fact is of little importance (whenever converged results were reached, their error with respect to the exact results was only a fraction of percent), the difference is easily perceptible. Thus for example, the converged results for central deflection, as predicted by the Q45-54 elements in Table 5.10, are 1.5084, 1.5069 and 1.5056 for the meshes 2×2, 4×4 and 8×8 respectively, while the exact value is 1.5046 (as invariably obtained with the same meshes from the *p*-extension process based on the Qab-c/d elements).

Table 5.10. Uniformly loaded square plate (*L/t*=10) with clamped boundaries. Comparison of solutions with incomplete (Qab-c) and T-complete (Qab-c/d) Trefftz function sets.

Quantity	Mesh	*M*=0		*M*=3		*M*=6		*M*=9		Exact
		Q21-11	Q21-9/1	Q32-21	Q32-17/5	Q43-33	Q43-25/9	Q54-45	Q54-33/13	
$\frac{10^2 D w_c}{\bar{q} L^4}$	1×1	1.5634	1.5634	1.4882	1.4959	1.5131	1.5080	1.5106	1.5048	1.5046
	2×2	1.4801	1.4793	1.5072	1.5036	1.5084	1.5048	1.5084	1.5046	
	4×4	1.5012	1.5004	1.5066	1.5045	1.5069	1.5046	1.5069	1.5046	
	8×8	1.5039	1.5034	1.5056	1.5046	1.5056	1.5046	1.5056	1.5046	
$\frac{10^2 M_{xc}}{\bar{q} L^2}$	1×1	3.4722	3.4722	2.3723	2.5264	2.3336	2.3112	2.3378	2.2664	2.3200
	2×2	2.3323	2.3237	2.3154	2.3214	2.3246	2.3240	2.3238	2.3194	
	4×4	2.3278	2.3274	2.3214	2.3201	2.3222	2.3201	2.3222	2.3200	
	8×8	2.3214	2.3209	2.3209	2.3200	2.3210	2.3200	2.3210	2.3200	
$-\frac{10 Q_{xB}}{\bar{q} L}$	1×1	3.4401	3.4401	4.4703	5.8251	4.2173	4.3030	4.2560	3.7950	4.1219
	2×2	3.4447	3.8340	4.2143	4.4136	4.2668	4.0889	4.2165	4.1134	
	4×4	3.6970	3.7993	4.1723	4.1448	4.1945	4.1234	4.1740	4.1219	
	8×8	3.9027	3.9366	4.1433	4.1216	4.1495	4.1233	4.1432	4.1219	

5.9.5 Uniformly loaded square plate with two edges free and the remaining two edges simply supported (Fig. 5.2d)

The results for *L/t*=10 and the percentage errors for *L/t*=10 and *L/t*=40 are displayed in Tables 5.13-5.15. Because of the unconstrained tangent rotations along a part of the boundary, this example exhibits along the two free edges a strong boundary layer effect of a similar nature to that shown in the case of soft simple support, SS1, in Section 5.8.3. It is therefore not surprising that the properties of the Qab-c and Qab-c/d solutions reported for soft simple support

Table 5.11. Uniformly loaded square plate (L/t=10) with clamped boundaries. Percent errors of solutions with incomplete (Qab-c) and T-complete (Qab-c/d) Trefftz function sets.

Quantity	Mesh	M=0		M=3		M=6		M=9	
		Q21-11	Q21-9/1	Q32-21	Q32-17/5	Q43-33	Q43-25/9	Q54-45	Q54-33/13
Δw_c%	1×1	3.91	3.91	–1.09	–0.58	0.56	0.23	0.40	0.01
	2×2	–1.63	–1.68	0.17	–0.07	0.25	0.01	0.25	0.00
	4×4	–0.23	–0.28	0.13	–0.01	0.15	0.00	0.15	
	8×8	–0.05	–0.08	0.07	0.00	0.07		0.07	
ΔM_{xc}%	1×1	49.66	49.66	2.25	8.90	0.59	–0.38	0.77	–2.31
	2×2	0.53	0.16	–0.20	0.06	0.20	0.17	0.16	–0.03
	4×4	0.34	0.32	0.06	0.00	0.09	0.00	0.09	0.00
	8×8	0.06	0.02	0.04		0.04		0.04	
ΔQ_{xB}%	1×1	–16.54	–16.54	8.45	41.32	2.31	4.39	3.25	–7.93
	2×2	–16.43	–6.98	2.24	7.08	3.52	–0.80	2.30	–0.21
	4×4	–10.31	–7.83	1.22	0.56	1.76	0.04	1.26	0.00
	8×8	–5.32	–4.50	0.52	–0.01	0.67	0.03	0.52	

Table 5.12. Uniformly loaded square plate (L/t=40) with clamped boundaries. Percent errors of solutions with incomplete (Qab-c) and T-complete (Qab-c/d) Trefftz function sets.

Quantity	Mesh	M=0		M=3		M=6		M=9	
		Q21-11	Q21-9/1	Q32-21	Q32-17/5	Q43-33	Q43-25/9	Q54-45	Q54-33/13
Δw_c%	1×1	0.36	0.36	–1.63	–0.26	0.15	0.07	0.00	0.03
	2×2	–4.04	–4.03	–0.10	–0.08	0.01	0.01	0.00	0.00
	4×4	–0.88	–0.87	0.00	0.00	0.01	0.00	0.01	
	8×8	–0.18	–0.18	0.01		0.01		0.01	
ΔM_{xc}%	1×1	54.23	54.23	4.37	6.64	–0.47	–9.07	–0.06	1.27
	2×2	–3.68	–4.12	–0.06	0.07	–0.03	–0.35	0.01	0.00
	4×4	–0.05	0.03	0.00	0.02	0.00	0.00	0.00	
	8×8	0.02	0.02		0.00				
ΔQ_{xB}%	1×1	–19.23	–19.23	10.17	670.68	–1.16	174.47	1.69	28.43
	2×2	–17.68	90.03	–0.38	149.37	1.60	7.26	0.75	–6.60
	4×4	–10.44	–1.91	0.53	21.28	1.64	–2.05	0.76	–1.59
	8×8	–5.95	–5.06	0.80	2.41	1.01	–0.25	0.61	–0.04

also apply to the present case. Indeed, the p-extension process based on the Qab-c/d T-complete set elements converges toward the exact solution, provided that the FE mesh has a certain minimum density (1×1 for L/t=10 and 4×4 for L/t=40 in the present case). Furthermore, the h-extension process with either of the two element types converges toward the exact solution and once more, if the Qab-c elements are used, the simplest of them, the Q21-11 element, yields the best results.

Table 5.13. Comparison of solutions with incomplete (Qab-c) and T-complete (Qab-c/d) Trefftz function sets for square plate as shown in Fig. 5.2d (L/t=10).

Quantity	Mesh	M=0		M=3		M=6		M=9		Exact
		Q21-11	Q21-9/1	Q32-21	Q32-17/5	Q43-33	Q43-25/9	Q54-45	Q54-33/13	
$\frac{10^2 D w_B}{\bar{q} L^4}$	1×1	1.7159	1.6491	1.6398	1.5804	2.2060	1.5632	2.9182	1.5607	1.5600
	2×2	1.5823	1.5732	1.5950	1.5622	1.6600	1.5598	1.7914	1.5600	
	4×4	1.5634	1.5594	1.5733	1.5601	1.5963	1.5600	1.6269	1.5600	
	8×8	1.5605	1.5588	1.5643	1.5600	1.5712	1.5600	1.5845	1.5600	
$\frac{10^2 M_{xc}}{\bar{q} L^2}$	1×1	1.4343	5.7816	2.6036	3.3280	2.2370	1.6064	1.2183	2.3008	2.5639
	2×2	2.6650	2.6833	2.2864	2.5959	2.0110	2.5673	1.6920	2.5624	
	4×4	2.5732	2.5950	2.4688	2.5669	2.3751	2.5640	2.2676	2.5639	
	8×8	2.5681	2.5772	2.5344	2.5642	2.5054	2.5639	2.4394	2.5639	
$-\frac{10 Q_{yD}}{\bar{q} L}$	1×1	3.1635	–5.9682	6.7957	6.4079	7.3974	1.0337	1.9047	4.2774	4.6497
	2×2	4.2438	4.0143	4.5763	4.6418	4.3890	1.2504	4.3613	4.6417	
	4×4	4.3549	4.3452	4.6154	4.6372	4.5915	1.2752	4.5581	4.6497	
	8×8	4.4984	4.5004	4.6403	4.6474	4.6320	1.2762	4.6119	4.6597	

Table 5.14. Percent errors of solutions with incomplete (Qab-c) and T-complete (Qab-c/d) Trefftz function sets for square plate as shown in Fig. 5.2d (L/t=10).

Quantity	Mesh	M=0		M=3		M=6		M=9	
		Q21-11	Q21-9/1	Q32-21	Q32-17/5	Q43-33	Q43-25/9	Q54-45	Q54-33/13
Δw_B%	1×1	9.99	5.71	5.11	1.31	41.41	0.20	87.06	0.04
	2×2	1.43	0.85	2.24	0.14	6.41	–0.01	14.83	0.00
	4×4	0.22	–0.04	0.85	0.01	2.33	0.00	4.29	
	8×8	0.03	–0.08	0.27	0.0	1.10		1.57	
ΔM_{xc}%	1×1	–44.06	125.50	1.55	29.80	–12.75	–37.35	–52.48	–10.26
	2×2	3.94	4.66	–10.82	1.25	–20.57	0.13	–34.01	–0.06
	4×4	0.36	1.21	–3.71	0.12	–7.37	0.00	–11.56	0.00
	8×8	0.16	0.52	–1.15	0.01	–2.28		–4.86	
ΔQ_{yD}%	1×1	–31.93	–228.36	46.15	37.81	59.09	47.18	–99.59	–8.01
	2×2	–8.73	–13.67	–1.58	–0.17	–5.61	0.38	–6.20	–0.17
	4×4	–6.34	–6.55	–0.74	–0.27	–1.25	0.00	–1.97	0.00
	8×8	–3.23	–3.21	–0.20	–0.05	–0.38		–0.81	

5.9.6 Uniformly loaded square plate on a Winkler type foundation with hard simple support (Fig. 5.2b)

For the purpose of comparison with Frederick's solution [2], the following parameters are used in the present calculation:

$$E = 206700\,\text{MPa}, \quad \mu = 0.3\,, \quad \bar{q} = 28.9\,\text{Mpa}\,, \quad L\text{=1.016 m.}$$

Table 5.16 shows the deflection at the centre of the plate using the element described in Section 5.6 for several values of t/L and the modulus of k_w. It can be

seen from the table that the results are in good agreement with the known ones. As expected, it is also found from the numerical results that the central deflection converges gradually to the exact result along with refinement of the element meshes.

Table 5.15. Percent errors of solutions with incomplete (Qab-c) and T-complete (Qab-c/d) Trefftz function sets for square plate as shown in Fig. 5.2d (L/t=40).

Quantity	Mesh	M=0		M=3		M=6		M=9	
		Q21-11	Q21-9/1	Q32-21	Q32-17/5	Q43-33	Q43-25/9	Q54-45	Q54-33/13
Δw_B%	1×1	11.01	7.11	3.26	3.71	29.13	23.86	80.93	18.02
	2×2	2.01	1.60	1.27	1.04	6.42	2.28	14.54	0.53
	4×4	0.47	0.32	0.68	0.24	2.59	0.09	4.47	0.01
	8×8	0.08	–0.01	0.39	0.03	1.09	0.00	1.48	0.00
ΔM_{xc}%	1×1	–44.34	–31.31	–12.13	–30.09	–114.21	–153.33	–430.04	84.27
	2×2	0.93	11.04	–8.47	8.77	–20.08	–21.63	–32.85	–0.05
	4×4	–0.47	0.25	–2.97	0.56	–7.69	–0.28	–9.90	–0.01
	8×8	–0.02	0.24	–1.39	0.02	–3.22	–0.01	–4.00	0.00
ΔQ_{yD}%	1×1	–32.77	–415.42	66.24	1204.11	145.78	1964.14	–611.82	–4950.88
	2×2	–8.87	–141.08	–0.40	82.49	–3.19	132.00	–6.87	–9.95
	4×4	–6.17	–16.17	–1.47	2.35	–1.41	0.02	–1.77	0.01
	8×8	–3.29	–3.71	–0.53	–0.13	–0.56	0.00	–0.70	0.00

Table 5.16. Central deflection of HT FE results and comparison with Frederick's solution [2].

Modulus k_w (10^5N/m^3)	t/L	[2] w_c(mm)	HT FE solution w_c(mm) 2×2	4×4	6×6
54.25	0.3	0.8153	0.8038	0.8122	0.8154
	0.2	2.2896	2.2765	2.2801	2.2896
	0.1	15.9990	15.4230	15.6520	15.9870
	0.05	117.4630	118.3230	117.9420	117.6250
542.5	0.3	0.8125	0.8201	0.8173	0.8129
	0.2	2.2669	2.2701	2.2702	2.2688
	0.1	14.9530	15.1180	15.0950	15.0230
	0.05	77.6110	78.5350	77.9990	77.8920
5425	0.3	0.7846	0.7913	0.7892	0.7858
	0.2	2.0625	2.0689	2.0658	2.0615
	0.1	9.0424	9.0551	9.0483	9.0472
	0.05	17.6680	17.9210	17.7030	17.6790

References

[1] Aminpour, M.A. Direct formulation of a hybrid 4-node shell element with drilling degrees of freedom. *Int. J. Numer. Meth. Eng*., **35**, pp. 997-1013, 1992.

[2] Frederick, D. Thick rectangular plates on elastic foundation. *Trans. ASCE*, **122**, pp. 1069-1085, 1957.

[3] Herrera, I. *Boundary Method: An algebraic theory*, Pitman: Boston, 1984.

[4] Hu, H.C. On some problems of the antisymmetrical small deflection of isotropic sandwich plate. *Acta Mechanica Sinica*, **6**, pp. 53-60, 1963 (in Chinese).

[5] Ibrahimbergovic, A. Quadrilateral finite elements for analysis of thick and thin plates. *Compu. Meth. Appl. Mech. Eng*., **110**, pp. 195-209, 1993.

[6] Jirousek, J. Hybrid-Trefftz plate bending elements with *p*-method capabilities. *Int. J. Numer. Meth. Eng*., **24**, pp. 1367-1393, 1987.

[7] Jirousek, J. Variational formulation of two complementary hybrid-Trefftz FE models. *Comm. Appl. Numer. Meth*., **9**, pp. 837-845, 1993.

[8] Jirousek, J. & Guex, L. The hybrid-Trefftz finite element model and its application to plate bending. *Int. J. Numer. Meth. Eng*., **23**, pp. 651-693, 1986.

[9] Jirousek, J. & Venkatesh, A. Hybrid-Trefftz plane elasticity elements with *p*-method capabilities. *Int. J. Numer. Meth. Eng*., **35**, pp. 1443-1472, 1992.

[10] Jirousek, J., Wroblewski, A., Qin, Q.H. & He, X.Q. A family of quadrilateral hybrid-Trefftz *p*-elements for thick plate analysis. *Compu. Meth. Appl. Mech. Eng*., **127**, pp. 315-344, 1995.

[11] Jirousek, J., Wroblewski, A. & Szybinski, B. A new 12 DOF quadrilateral element for analysis of thick and thin plates. *Int. J. Numer. Meth. Eng*., **38**, pp. 2619-2638, 1995.

[12] Mindlin, R.D. Influence of rotatory inertia and shear on flexural motion of isotropic elastic plates. *J. Appl. Mech*., **18**, pp. 31-38, 1951.

[13] Panc, V. *Theories of Elastic Plates*, Noordhoff: Leidin, 1975.

[14] Petrolito, J. Hybrid-Trefftz quadrilateral elements for thick plate analysis. *Compu. Meth. Appl. Mech. Eng*., **78**, pp. 331-351, 1990.

[15] Petrolito, J. Triangular thick plate elements based on a Hybrid-Trefftz approach. *Compu. Struct*., **60**, pp. 883-894, 1996.

[16] Qin, Q.H. Nonlinear analysis of Reissner plates on an elastic foundation by BEM. *Int. J. Solids Struct*., **30**, pp. 3101-3111, 1993.

[17] Qin, Q.H. Hybrid-Trefftz finite element method for Reissner plates on an elastic foundation. *Compu. Meth. Appl. Mech. Eng*., **122**, pp. 379-392, 1995.

[18] Qin, Q.H. Nonlinear analysis of thick plates by HT FE approach. *Compu. Struct*., **61**, pp. 271-281, 1996.

[19] Qin, Q.H. & Diao S. Nonlinear analysis of thick plates on an elastic foundation by HT FE with p-extension capabilities. *Int. J. Solids Struct*., **33**, pp. 4583-4604, 1996.

[20] Reismann, H. *Elastic Plates: Theory and applications*, Wiley: New York, 1988.

[21] Reissner, E. The effect of shear deformation on the bending of elastic plates. *J. Appl. Mech*., **12**, pp. 69-76, 1945.
[22] Taylor, R.L. & Auricchio, F.A. Linked interpolation for Reissner-Mindlin plate elements: Part II—A simple triangle. *Int. J. Numer. Meth. Eng*., **36**, pp. 3057-3066, 1993.
[23] Xu, Z. A simple and efficient triangular finite element for plate bending. *Acta Mechanica Sinica*, **2**, pp. 185-192, 1986.
[24] Xu, Z. A thick-thin triangular plate element. *Int. J. Numer. Meth. Eng*., **33**, pp. 963-973, 1992.
[25] Zienkiewicz, O.C. & Taylor, R.L. *The Finite Element Method*, 4th edn, McGraw Hill: London, 1989.
[26] Zienkiewicz, O.C., Xu, Z., Zeng, L.F., Samuelson, A. & Wiberg, N.E. Linked interpolation for Reissner-Mindlin plate elements: Part I—A simple quadrilateral. *Int. J. Numer. Meth. Eng*., **36**, pp. 3043-3056, 1993.